Environmental Pollution 240 (2018) 353–358

Contents lists available at ScienceDirect

Environmental Pollution

journal homepage: www.elsevier.com/locate/envpol

Lidar mapping of atmospheric atomic mercury in the Wanshan area, China☆

Ming Lian [a], Lihai Shang [b], Zheng Duan [a], Yiyun Li [a], Guangyu Zhao [a], Shiming Zhu [a], Guangle Qiu [b], Bo Meng [b], Jonas Sommar [b], Xinbin Feng [b, **], Sune Svanberg [a, c, *]

[a] Center for Optical and Electromagnetic Research, South China Academy of Advanced Optoelectronics, Science Building 5, South China Normal University, University City Campus, Guangzhou 510006, China
[b] State Key Laboratory of Environmental Geochemistry, Institute of Geochemistry, Chinese Academy of Sciences, Guiyang 550081, China
[c] Department of Physics, Lund University, P.O. Box 118, SE-221 00 Lund, Sweden

ARTICLE INFO

Article history:
Received 11 January 2018
Received in revised form
26 March 2018
Accepted 23 April 2018

Keywords:
Differential absorption lidar
Wanshan
Gaseous atomic mercury
Concentration mapping

ABSTRACT

A novel mobile laser radar system was used for mapping gaseous atomic mercury (Hg^0) atmospheric pollution in the Wanshan district, south of Tongren City, Guizhou Province, China. This area is heavily impacted by legacy mercury from now abandoned mining activities. Differential absorption lidar measurements were supplemented by localized point monitoring using a Lumex RA-915M Zeeman modulation mercury analyzer. Range-resolved concentration measurements in different directions were performed. Concentrations in the lower atmospheric layers often exceeded levels of 100 ng/m^3 for March conditions with temperature ranging from 5 °C to 20 °C. A flux measurement of Hg^0 over a vertical cross section of 0.12 km^2 resulted in about 29 g/h. Vertical lidar sounding at night revealed quickly falling Hg^0 concentrations with height. This is the first lidar mapping demonstration in a heavily mercury-polluted area in China, illustrating the lidar potential in complementing point monitors.

1. Introduction

Mercury is a neurotoxic heavy metal pollutant. Metallic mercury has a high vapor pressure and, in the atmosphere, it largely remains in gaseous atomic form (Hg^0) and can spread easily through air transportation (Beckers and Rinklebe, 2017; Mazzolai et al., 2004; Rinklebe et al., 2010). Mercury is now the target of the UN's Minamata Convention legally entered into force in 2017 (United Nations, 2013). China, one of the signatory countries, is a major producer and user of mercury and much attention is paid to its study and mitigation in the environment (Feng, 2005; Feng and Qiu, 2008; Fu et al., 2012; Streets et al., 2005; Zhang and Wong, 2007). The mercury emissions of anthropogenic origin in China are estimated to be more than 500 tons annually (Streets et al., 2005). The Guizhou province is rich in mercury minerals, and mining activities in the Wanshan area of Eastern Guizhou have been ongoing since the Qin Dynasty, about 200 BC. Known as the Chinese mercury capital, Wanshan was the largest mercury mine in China up till the official close-down of the activities in 2002. However, some non-official artisanal activities have been ongoing since then, causing a substantial detrimental environmental impact. The study of mercury in the Wanshan area using point monitors has been extensive; see e.g. (Dai et al., 2012; Du et al., 2016; Feng et al., 2008; Li et al., 2009; Qiu et al., 2008).

The Wanshan mercury ore deposit is part of the global belt of cinnabar (HgS) mineralization, which has a large extension. In Europe, Almaden (Spain), Abbadia San Salvatore (Italy) and Idrija (Slovenia) are sites of historically major mercury extraction. The fact that atmospheric mercury is largely in atomic form while all other gaseous pollutants are molecular results in a unique possibility for extremely sensitive optical mercury detection, down to the Northern hemispherical background concentration in the range 1.3–1.6 ng/m^3 (Sprovieri et al., 2016). Then the differential absorption lidar (DIAL) technique becomes very useful for range-resolved concentration measurements (Svanberg, 1994).

☆ This paper has been recommended for acceptance by Dr. Jorg Rinklebe.

* Corresponding author. Center for Optical and Electromagnetic Research, South China Academy of Advanced Optoelectronics, Science Building 5, South China Normal University, University City Campus, Guangzhou 510006, China.
** Corresponding author. State Key Laboratory of Environmental Geochemistry, Institute of Geochemistry, Chinese Academy of Sciences, Guiyang 550081, China.
E-mail addresses: Fengxinbin@vip.skleg.cn (X. Feng), sune.svanberg@fysik.lth.se (S. Svanberg).

https://doi.org/10.1016/j.envpol.2018.04.104
0269-7491/

The lidar group of Lund University, Sweden, has performed extensive studies on atmospheric Hg^0. The total flux from the electrolytic cell houses of chlor-alkali industries, where Hg^0 is used as an electrode in the electrolytic baths producing sodium hydroxide, has been determined (Grönlund et al., 2004, 2005b). Further, the mapping of Hg^0 in Icelandic and Italian thermal fields has been pursued (Edner et al., 1991, 1992). As part of a larger program of studies of gases of geophysical origin (Svanberg, 2002), lidar mapping of atomic mercury at all major European mercury mines was performed (Edner et al., 1993; Ferrara et al., 1998; Grönlund et al., 2005a).

DIAL is widely used in the measurement of various kinds of gases, including O_3, CO_2, and CH_4 (Burlakov et al., 2010; Innocenti et al., 2017; Koch et al., 2004). However, the measurement of gaseous atomic mercury requires very specialized equipment and had only been pursued by the Lund university group. With the cessation of this research direction in Lund, the South China Normal University group is now the only group world-wide which can perform such measurement. Along these lines, the present paper now reports the first DIAL study of Hg^0 in a heavily mercury-polluted area in China. The demonstration shows the substantial potential of this technology in complementing customary point monitoring studies and could provide a new dimension in the management of the serious mercury pollution in certain areas of Asia.

2. Mobile lidar system description

An advanced mobile lidar system has just been constructed at South China Normal University, Guangzhou with the prime purpose of atomic mercury monitoring on the Chinese scene (Zhao et al., 2017). The measurements of atmospheric Hg^0 in the Wanshan mining area reported here were conducted using this system, which is shown in photographs in Fig. 1 on a site close to the Wanshan city center (27° 31′ 23.0″ N, 109° 12′ 41.3″ E). This location was chosen because of being in the residential area where the population is subjected to the pollution, and because of the convenient availability of three-phase electrical power.

A detailed description of the system can be found in (Zhao et al., 2017). Here only a brief overview of the system is given. Equipped with a Nd:YAG laser, the system can emit laser radiation at a pulse repetition rate of 20 Hz at the primary wavelength of 1064 nm, with harmonics at 532 nm, 355 nm and 266 nm as generated in phase-matched non-linear crystals. When pumping the tunable dye laser supplied with the system, intense pulses of a wide range of wavelengths can be obtained. In particular, about 10 mJ/pulse of radiation at the atomic mercury absorption line close to 253.7 nm can be attained by frequency doubling of the dye laser radiation generated when using the dye Coumarin 307. A 40-cm–diameter receiving Newtonian telescope is used to collect back-scattered radiation. A stepping motor-driven roof-top mirror is used for deflecting the vertically transmitted beam and the field of view of the co-axially arranged telescope, allowing the direction of measurement to be changed 360° horizontally and the elevation angle to be adjusted between −10° and 45°.

Using a piezo-electric fast-wavelength switching arrangement, the wavelength could for every other transmitted pulse be changed from the Hg^0 absorption line to an adjacent non-absorbed wavelength, while avoiding the influence of near-by molecular oxygen lines, as discussed in (Mei et al., 2014). Signals in the form of lidar transients for the two wavelengths could then be digitized and averaged over many laser pulses to attain the necessary signal-to-noise ratio, to allow a range-resolved concentration evaluation from the ratio curve (Svanberg, 1994). The attainable range is limited by the $1/R^2$ signal fall-off for lidars operating in back-scattering mode. The whole system, including the setting of measurement directions, is controlled in LabVIEW software installed in the system computers, which also visualize the signal collected. A quasi–real-time data evaluation program is developed in MATLAB. In our data evaluation, an atomic mercury differential absorption cross-section of $2.5*10^{-14}$ cm^2/atom was adopted, as discussed in Mei et al. (2014).

3. Measurements and results

3.1. Introduction to the measurements

Fig. 2 is an overview of the measurement area. The mobile system was parked approximately, 600 m west of the border to the National Mining Park of Wanshan, which is the site of abandoned ancient mercury mines. Differential absorption lidar recordings are illustrated in Fig. 3 which were obtained from measurement direction A as indicated in Fig. 2 (a) and with an elevation angle of about 20°. In Fig. 3 (a), a pair of on- and off-resonance lidar recordings is shown with different scales at different distances, (b) shows the on/off ratio (DIAL) curve and the correspondingly evaluated concentration. Identical on/off curves, resulting in a constant ratio of 1.00, would correspond to the complete absence of absorbing Hg^0. Instead, the curve in (b) is clearly sloping with different inclinations, from which the range-resolved atomic mercury concentration is evaluated. Fluctuating and frequently very high Hg^0 concentrations were observed in this heavily polluted area.

Although the typical detection distance of our system for Hg^0 is roughly 1 km, reliable data obtained in the Wanshan area normally were available only out to a distance of about 700 m. One reason is the heavy absorption of the on-resonance lidar curve due to the exceedingly high concentrations in the local atmosphere. We further by routine reject the data recorded from ranges shorter than 100 or 150 m, since they may be compromised by the very high

Fig. 1. The South China Normal University mobile system operating on site in Wanshan for monitoring of atmospheric atomic mercury.

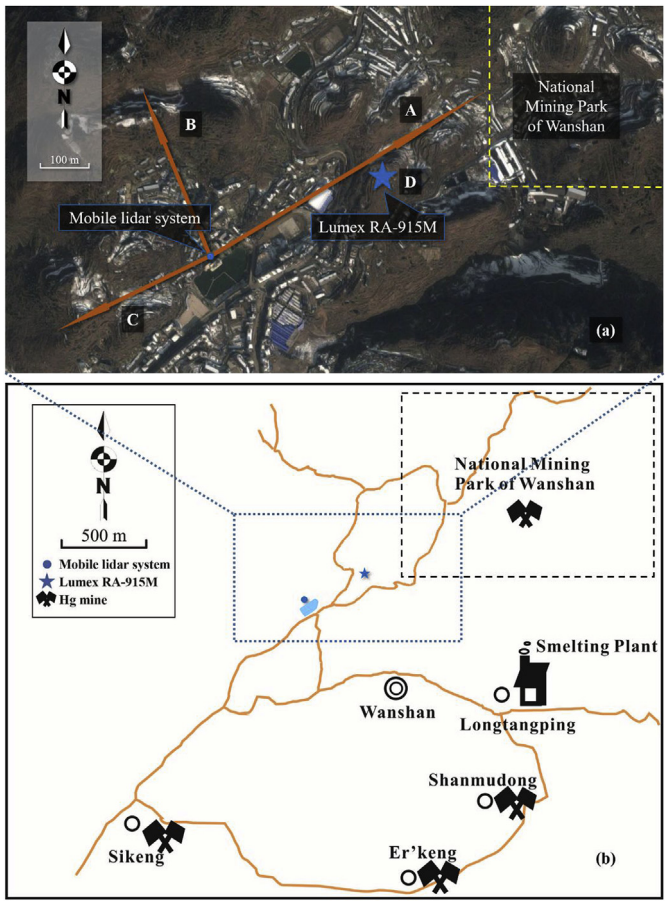

Fig. 2. Overviews of the measurement area. The three detection directions are indicated in (a) as A (59°), B (338°) and C (244°). Point D (marked as a blue star) is the position of the Lumex RA-915M mercury analyzer when the instrumental intercomparison experiment was performed. Certain structures specially related to mercury mining are indicated in (b), which covers a larger area. (For interpretation of the references to colour in this figure legend, the reader is referred to the Web version of this article.)

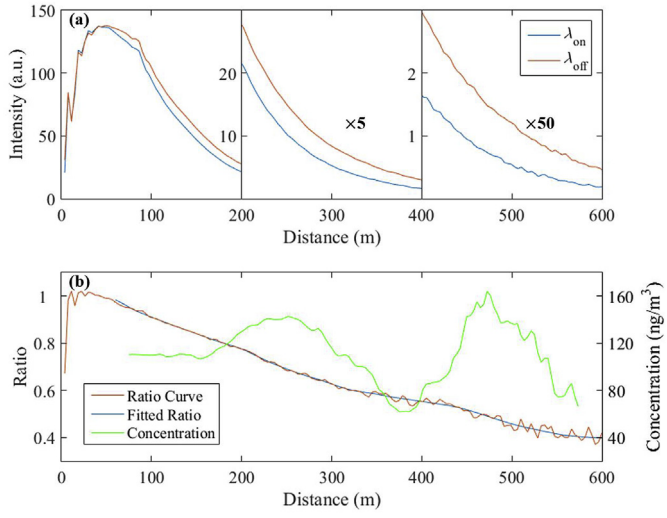

Fig. 3. (a) shows on- and off-resonance lidar recordings of atmospheric backscatter; (b) displays the resulting ratio curve and the evaluated range-resolved concentration values. Concentrations were evaluated with a 100-m sliding average routine. Data were integrated for 1 min.

close-range back-scattered intensities in combination with increased sensitivity to slight optical misalignments at short ranges. However, close-range data can clearly be obtained with an on-site point monitoring system.

Actually, during the field experiments, a Hg^0 point concentration monitor (Model RA-915M, Lumex Instruments) was available, operating on the principle of Zeeman modulation of the same 253.7 nm monitoring line as was used in the DIAL measurements. This instrument is from the same series as was used, e.g. in the studies reported in Dai et al. (2012) and Grönlund et al. (2005a). In order to connect to the substantial work previously reported from the Wanshan area with point monitors, we performed an instrumental inter-comparison experiment. This is the first time that a Zeeman modulated point monitor has been inter-calibrated to DIAL. The laser beam was aimed at about 2 m above the top of the hill slightly to the right of direction A (position D), while the Lumex mercury analyzer was placed on the ground, right beneath the laser beam, simultaneously recording the Hg^0 concentration at that point (Fig. 4).

The result is displayed in Fig. 5. Panel (a) shows a pair of lidar curves obtained during this session. When amplified, tiny bumps are distinguished at the distance of 420 m, which are the echoes of the green wire fence at the site (visible in Fig. 4 (a), (c)), thus indicating the location of the Lumex mercury analyzer — exactly like a laser range finder would do. The two groups of data, displayed in Fig. 4 (c), compare favourably, with a correlation coefficient of 0.95. If a linear regression is forced through the origin, the fitting function is $y = 1.101^*x$, with a 95% confidence bound of the slope to be between 1.045 and 1.157. In the fitting function, y and x stand for results of lidar and Lumex RA-915M, respectively. The observed deviation from a unity slope may be explained by the non-perfect overlap of the sites of measurements, or more likely, by the respectively chosen calibrations for the lidar and Lumex instruments, respectively. As mentioned, the determination of the value of the optical absorption cross-section of mercury near 253.7 nm has not reached a consensus (Mei et al., 2014). If it is assumed that the Lumex device is accurately calibrated and related to other standard point monitoring devices such as TEKRAN and GARDIS, it can be treated as the standard device and correspondingly adjust the lidar differential absorption cross section setting in our data processing program, which would then, according to the fit in Fig. 5 (c), result in about 9 percent lower mercury concentrations compared to the reported DIAL values, bringing them into full accordance with Lumex.

3.2. Vertical scan in three different directions

Since the system was positioned in a valley, the surrounding mountains and buildings leave us limited directions accessible to probe. Three feasible directions are indicated as A, B, and C in Fig. 2 (a). We performed vertical scans, and evaluated data are shown in Fig. 6. The elevations were chosen between 15° and 36°, with an increment of 3° between the measurement directions.

The results show a great difference in Hg^0 concentration in different directions. The maximum value in direction A was over 120 ng/m^3, while in the other two directions no more than 50 ng/m^3 was observed. The National Mining Park is a relic of former operating mines, and the atmospheric mercury concentration in that direction was considerably higher than in the other two directions, suggesting that it is still a major source for mercury pollution to the air.

Combined with wind data, the results can be used to deduce the mercury flux through the monitored areas. A weather station was installed on a near-by roof about 10 m above the ground, which recorded wind speed as well as other weather information. As for

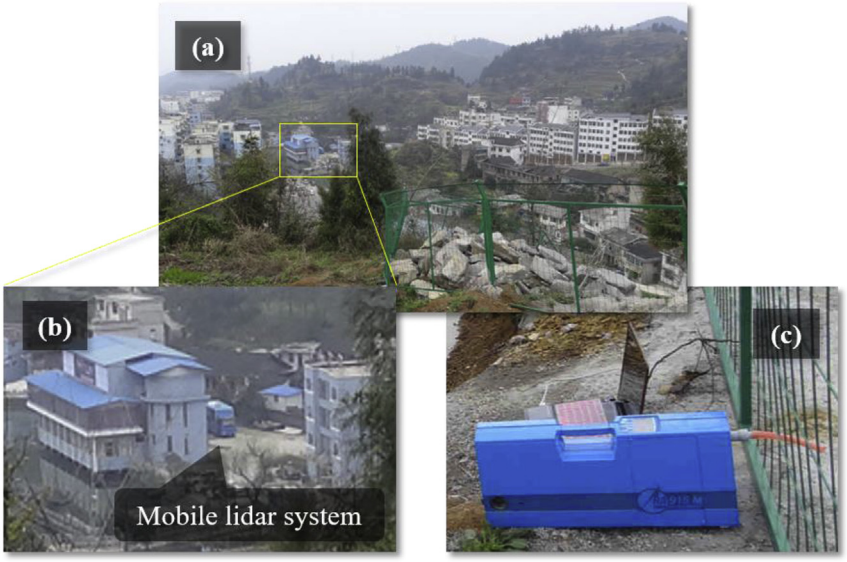

Fig. 4. (a): an overlook at the mobile lidar system as seen from position D; (b): an enlargement showing the mobile lidar system as seen from position D; (c): the Lumex RA-915M mercury analyzer operating at position D.

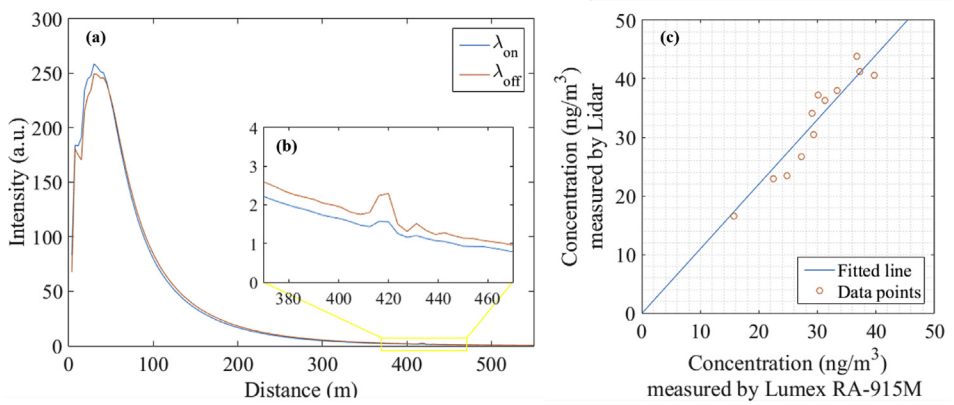

Fig. 5. The inter-comparison between data recorded by lidar and Lumex RA-915M. Panel (a) is one sample of lidar curve obtained; inset (b) displays the faint echo of the wire fence at position D, defining the accurate location of the Lumex instrument; scatter plot (c) combines two groups of Hg^0 concentration data with the associated linear fitting through the origin.

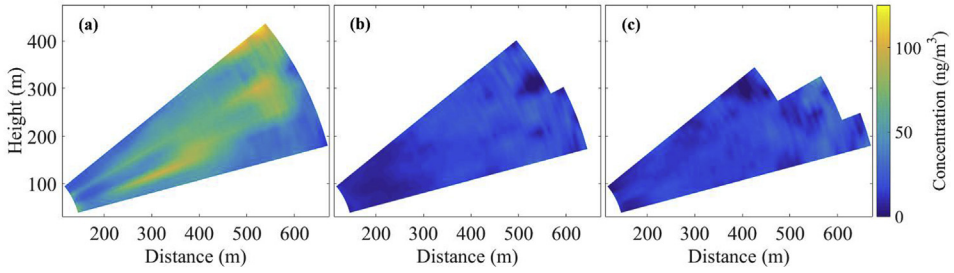

Fig. 6. Vertical scans in the three directions indicated as A, B, and C in Fig. 2. High Hg^0 concentrations were found particularly in direction A, towards the abandoned mercury mines.

the 12-min section depicted in Fig. 6 (a), the average wind speed was about 1.4 m/s, from direction 135° (southeast); while the direction of the measurement was 60°, meaning a perpendicular wind speed of 1.35 m/s. The total flux for the scanned $1.2*10^5$-m^2 area was then estimated to be 29 g/h. We note that for the wind conditions, the mercury plume from the Longtangping smelting plant, which is known as a strong mercury source, could be brought into the scanned area.

To further corroborate the result above, we performed another scan in direction A during the following night, with a smaller elevation angular step of 2°, from 15° to 39°. This session was associated with calm weather conditions: a near-zero wind was

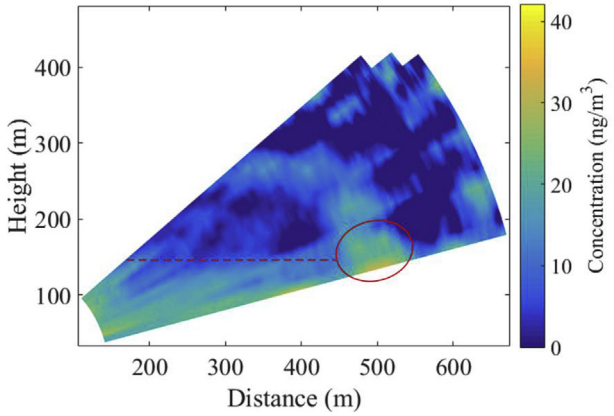

Fig. 7. The result of the second scan in direction A. The "hot zone" (red oval) indicates strong emission of mercury from the National Mining Park; the dashed line marks a height of about 150 m above which the Hg^0 concentration is considerably lower. (For interpretation of the references to colour in this figure legend, the reader is referred to the Web version of this article.)

measured by the weather station, and the lack of the heat provided by the sun leads to a low transport. Under such conditions, air in the surface layer tends to align to a stable vertical stratification leading to that turbulent mixing declines and pronounced concentration gradients may emerge above a surface source. Consequently, nocturnal Hg^0 scanning may facilitate a detailed mapping of the distribution of terrestrial sources of legacy mercury, and possibly be useful for exploration purposes, to be discussed later.

The measurement results (Fig. 7) show that the overall Hg^0 concentration was considerably lower than during the first measurement (Fig. 6 (a)) conducted at daytime. The main reason is that the surface evaporation of Hg^0 displays a strong temperature dependence. When the temperature decreased from 14 °C at daytime to 7 °C at night, the mercury vapor pressure decreased by a factor of 0.5 over metallic mercury residues (Huber et al., 2006), which are widespread in connection with the ore roasting and in the roasted cinnabar tailings. Also, the contribution of the plume from the Longtangping smelting plant was absent. The concentrations from the height of 50 m–150 m ranged from 20 to 30 ng/m^3, and were relatively homogeneous, while there was an obvious decrease above 150 m (the horizontal dashed line indicates this demarcation). However, over the area at about 500 m distance (the edge of the Mining Park), there was a "hot zone" (the oval). The maximum concentration inside the "hot zone" was over 40 ng/m^3, while it was mostly below 10 ng/m^3 in surrounding space. The result of the second scan confirmed that the National Mining Park of Wanshan is still emitting significant amounts of mercury. Unfortunately, we could not move the laser beam to lower elevations because of beam obstructions. Otherwise a more comprehensive profile of the "hot zone" could have been recorded.

3.3. Recordings of concentration variations over time

Besides vertical scanning, we also monitored range-resolved mercury concentrations over time along fixed directions, mostly with an elevation angle of about 25° in the measurement direction A shown in Fig. 2 (a). Examples of two data sets, each extending over about 1 h, are shown in Fig. 8. In particular, we note in (a) how the area of highest mercury concentration moved closer to the lidar system during the measurement session, presumably due to a successive change in wind direction bringing a localized plume from an emission source closer. Dramatic fluctuations of the mercury concentration are displayed in (b) with a maximum value of over 200 ng/m^3.

4. Discussion

The present measurement campaign is a demonstration of the capabilities of remote-sensing lidar monitoring of atomic mercury in a heavily polluted mining setting on the Chinese scene. Although a compromised site for the system deployment had to be chosen for logistic reasons in this first field mercury lidar experiment in Asia, the data obtained clearly demonstrate a considerable potential of the technique. In particular, the unique capability of total flux measurements of Hg^0 out from a given area as provided by DIAL mapping should be exploited. As a preview of such activities, we have shown that with the mercury concentration map given in Fig. 6 (a) and measured wind data, the total mercury flux through the probed area was around 29 g/h. We are now supplying the mobile system with a Diesel generator for providing power at any deployment site. We plan for such measurements in the direct vicinity of major Wanshan mining and processed cinnabar ore deposit sites, to assess their total contribution of mercury to the atmosphere for different environmental conditions.

Future applications of our mobile atomic mercury monitoring lidar system include emissions from industries and coal-burning power plants as well as from coal mines. As mentioned earlier, there are prospects to use atomic mercury as a tracer gas for geothermal energy resources and for possible valuable mineral localizations. The relation of observed mercury anomalies to the prediction of seismic and earthquake activities is a further potential aspect of efficient monitoring of the extremely volatile mercury gas. These aspects have been pointed out earlier (Edner et al., 1992; Jin

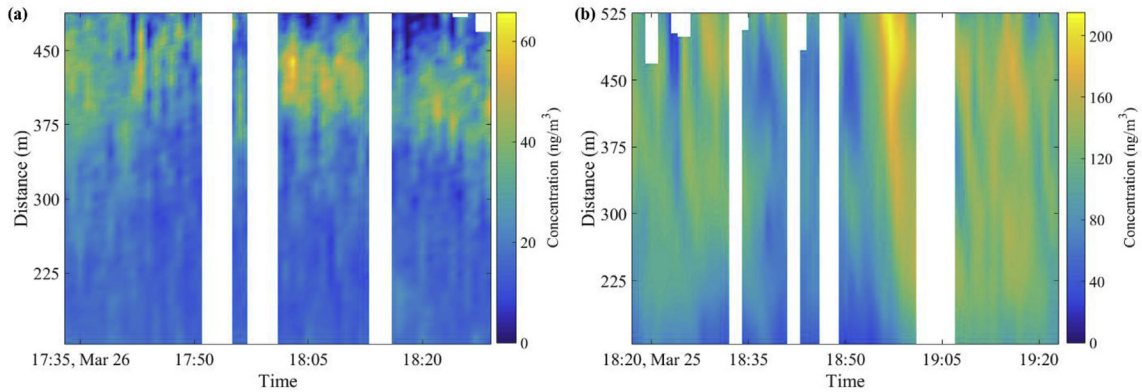

Fig. 8. Range-resolved mercury concentrations: (a) during March 26, and (b) during March 25, 2016.

et al., 1989; McCarthy et al., 1969), but are still awaiting the dedicated trials using a well-adapted system, such as the one described here. Actually, our mobile system has also already been deployed in a logistically similar and successful archeological study of considerable interest, regarding burial site mercury (Zhao et al., Unpublished results).

Acknowledgements

The authors gratefully acknowledge the support of Profs Sailing He and Guofu Zhou. This work was financially supported by a Guangdong Province Innovation Research Team Program (No. 201001D0104799318).

References

Beckers, F., Rinklebe, J., 2017. Cycling of mercury in the environment: sources, fate, and human health implications: a review. Crit. Rev. Environ. Sci. Technol. 47, 693–794.

Burlakov, V.D., Dolgii, S.I., Makeev, A.P., Nevzorov, A.V., Romanovskii, O.A., Kharchenko, O.V., 2010. A differential-absorption lidar for ozone sensing in the upper atmosphere-lower stratosphere. Instrum. Exp. Tech. 53, 886–889. https://doi.org/10.1134/S0020441210060229.

Dai, Z.H., Feng, X.B., Sommar, J., Li, P., Fu, X.W., 2012. Spatial distribution of mercury deposition fluxes in Wanshan Hg mining area, Guizhou province, China. Atmos. Chem. Phys. 12, 6207–6218.

Du, B., Li, P., Feng, X., Qiu, G., Zhou, J., Maurice, L., 2016. Mercury exposure in children of the Wanshan mercury mining area, Guizhou, China. Int. J. Environ. Res. Publ. Health 13 (1107). https://doi.org/10.3390/ijerph13111107.

Edner, H., Faris, G.W., Sunesson, A., Svanberg, S., Bjarnason, J.Ö., Kristmannsdóttir, H., Sigurdsson, K.H., 1991. Lidar search for atmospheric atomic mercury in Icelandic geothermal fields. J. Geophys. Res. 96, 2977–2986. https://doi.org/10.1029/90JD02350.

Edner, H., Ragnarson, P., Svanberg, S., Wallinder, E., De Liso, A., Ferrara, R., Maserti, B.E., 1992. Differential absorption lidar mapping of atmospheric atomic mercury in Italian geothermal fields. J. Geophys. Res. 97, 3779–3786. https://doi.org/10.1029/91JD03108.

Edner, H., Ragnarson, P., Svanberg, S., Wallinder, E., Ferrara, R., Maserti, B.E., Bargagli, R., 1993. Atmospheric mercury mapping in a cinnabar mining area. Sci. Total Environ. 133, 1–15. https://doi.org/10.1016/0048-9697(93)90110-R.

Feng, X., 2005. Mercury pollution in China — an overview. In: Pirrone, N., Mahaffey, K.R. (Eds.), Dynamics of Mercury Pollution on Regional and Global Scales. Springer, Boston, pp. 657–678. https://doi.org/10.1007/0-387-24494-8_27.

Feng, X., Li, P., Qiu, G., Wang, S., Li, G., Shang, L., Meng, B., Jiang, H., Bai, W., Li, Z., Fu, X., 2008. Human exposure to methylmercury through rice intake in mercury mining areas, Guizhou province, China. Environ. Sci. Technol. 42, 326–332. https://doi.org/10.1021/es071948x.

Feng, X., Qiu, G., 2008. Mercury pollution in Guizhou, Southwestern China — an overview. Sci. Total Environ. 400, 227–237. https://doi.org/10.1016/j.scitotenv.2008.05.040.

Ferrara, R., Maserti, E., Andersson, M., Edner, H., Ragnarson, P., Svanberg, S., Hernandez, A., 1998. Atmospheric mercury concentrations and fluxes in the Almadén district (Spain). Atmos. Environ. 32, 3897–3904. https://doi.org/10.1016/S1352-2310(98)00102-2.

Fu, X., Feng, X., Sommar, J., Wang, S., 2012. A review of studies on atmospheric mercury in China. Sci. Total Environ. 421–422, 73–81. https://doi.org/10.1016/J.SCITOTENV.2011.09.089.

Grönlund, R., Edner, H., Svanberg, S., Kotnik, J., Horvat, M., 2005a. Mercury emissions from the Idrija mercury mine measured by differential absorption lidar techniques and a point monitoring absorption spectrometer. Atmos. Environ. 39, 4067–4074. https://doi.org/10.1016/J.ATMOSENV.2005.03.027.

Grönlund, R., Sjöholm, M., Weibring, P., Edner, H., Svanberg, S., 2005b. Elemental mercury emissions from chlor-alkali plants measured by lidar techniques. Atmos. Environ. 39, 7474–7480. https://doi.org/10.1016/j.atmosenv.2005.06.060.

Grönlund, R., Sjöholm, M., Weibring, P., Edner, H., Svanberg, S., 2004. Mercury emissions from chlor-alkali plants measured by lidar techniques. RMZ Mater. Geoenviron 51, 1585.

Huber, M.L., Laesecke, A.R., Friend, D.G., 2006. The Vapor Pressure of Mercury, NIST Interagency/Internal Report (NISTIR), p. 6643.

Innocenti, F., Robinson, R., Gardiner, T., Finlayson, A., Connor, A., 2017. Differential absorption lidar (DIAL) measurements of landfill methane emissions. Rem. Sens. 9 (953). https://doi.org/10.3390/rs9090953.

Jin, Y., Wu, Z., Shen, C., Wei, J., Zhu, H., 1989. Earthquake prediction through the observation and measurement of mercury content variation in water. J. Geochem. Explor. 33, 195–202. https://doi.org/10.1016/0375-6742(89)90029-0.

Koch, G.J., Barnes, B.W., Petros, M., Beyon, J.Y., Amzajerdian, F., Yu, J., Davis, R.E., Ismail, S., Vay, S., Kavaya, M.J., Singh, U.N., 2004. Coherent differential absorption lidar measurements of CO_2. Appl. Optic. 43, 5092–5099. https://doi.org/10.1364/AO.43.005092.

Li, P., Feng, X., Qiu, G., Shang, L., Li, G., 2009. Human hair mercury levels in the Wanshan mercury mining area, Guizhou Province, China. Environ. Geochem. Health 31, 683–691. https://doi.org/10.1007/s10653-008-9246-x.

Mazzolai, B., Mattioli, V., Raffa, V., Tripoli, G., Dario, P., Ferrara, R., Lanzilotta, E., Munthe, J., Wängberg, I., Barregård, L., Sällsten, G., Horvat, M., Gibicar, D., Fajon, V., Logar, M., Pacyna, J., Denby, B., Svanberg, S., Edner, H., Grönlund, R., Sjöholm, M., Weibring, P., Donati, A., Baldacci, S., Vigann, W., Pannocchia, A., Fontanelli, R., la Manna, S., di Bona, S., Fudala, J., Zielonka, U., Hlawiczka, S., Jarosinska, D., Danet, A., Bratu, C., 2004. A mulitdisciplinary approach to study the impact of mercury pollution on human health and environment: the EMECAP project. RMZ Mater. Geoenviron 51, 682–682.

McCarthy, J.H., Vaughn, W.W., Learned, R.E., Meuschke, J.L., 1969. Mercury in Soil Gas and Air — a Potential Tool in Mineral Exploration, U.S. Geological Survey, Circular 609.

Mei, L., Zhao, G., Svanberg, S., 2014. Differential absorption lidar system employed for background atomic mercury vertical profiling in South China. Opt. Laser. Eng. 55, 128–135. https://doi.org/10.1016/j.optlaseng.2013.10.028.

Qiu, G., Feng, X., Li, P., Wang, S., Li, G., Shang, L., Fu, X., 2008. Methylmercury accumulation in rice (Oryza sativa L.) grown at abandoned mercury mines in Guizhou, China. J. Agric. Food Chem. 56, 2465–2468. https://doi.org/10.1021/jf073391a.

Rinklebe, J., During, A., Overesch, M., Du Laing, G., Wennrich, R., Stärk, H.J., Mothes, S., 2010. Dynamics of mercury fluxes and their controlling factors in large Hg-polluted floodplain areas. Environ. Pollut. 158, 308–318.

Sprovieri, F., Pirrone, N., Bencardino, M., D'Amore, F., Carbone, F., Cinnirella, S., Mannarino, V., Landis, M., Ebinghaus, R., Weigelt, A., Brunke, E.G., Labuschagne, C., Martin, L., Munthe, J., Wängberg, I., Artaxo, P., Morais, F., De Melo Jorge Barbosa, H., Brito, J., Cairns, W., Barbante, C., Del Carmen Diéguez, M., Elizabeth Garcia, P., Aurélien, D., Angot, H., Magand, O., Skov, H., Horvat, M., Kotnik, J., Alana Read, K., Mendes Neves, L., Manfred Gawlik, B., Sena, F., Mashyanov, N., Obolkin, V., Wip, D., Bin Feng, X., Zhang, H., Fu, X., Ramachandran, R., Cossa, D., Knoery, J., Marusczak, N., Nerentorp, M., Norstrom, C., 2016. Atmospheric mercury concentrations observed at ground-based monitoring sites globally distributed in the framework of the GMOS network. Atmos. Chem. Phys. 16, 11915–11935. https://doi.org/10.5194/acp-16-11915-2016.

Streets, D.G., Hao, J., Wu, Y., Jiang, J., Chan, M., Tian, H., Feng, X., 2005. Anthropogenic mercury emissions in China. Atmos. Environ. 39, 7789–7806. https://doi.org/10.1016/j.atmosenv.2005.08.029.

Svanberg, S., 2002. Geophysical gas monitoring using optical techniques: volcanoes, geothermal fields and mines. Opt. Laser. Eng. 37, 245–266. https://doi.org/10.1016/S0143-8166(01)00098-7.

Svanberg, S., 1994. Differential absorption lidar (DIAL). In: Sigrist, M. (Ed.), Air Monitoring by Spectroscopic Techniques. John Wiley, New York, p. 85.

United Nations, 2013. Minamata Convention on Mercury. http://www.mercuryconvention.org/Portals/11/documents/Booklets/Minamata%20Convention%20on%20Mercury_booklet_English.pdf.

Zhang, L., Wong, M.H., 2007. Environmental mercury contamination in China: sources and impacts. Environ. Int. 33, 108–121. https://doi.org/10.1016/J.ENVINT.2006.06.022.

Zhao, G. et al., Unpublished Results. Mercury Emission from the Emperor Qin Tomb in Xi'an Studied by Laser Radar.

Zhao, G., Lian, M., Li, Y., Duan, Z., Zhu, S., Mei, L., Svanberg, S., 2017. Mobile lidar system for environmental monitoring. Appl. Opt. 56, 1506–1516. https://doi.org/10.1364/AO.56.001506.